05

Magnetic properties of ultra-small $NiFe_2O_4$ nanoparticles system coated with PVA

© D.A. Balaev[1], A.A. Krasikov[1], D.A. Velikanov[1], S.V. Stolyar[1,2], A.O. Shokhrina[2], A.D. Balaev[1], R.S. Iskhakov[1]

[1] Kirensky Institute of Physics, Federal Research Center KSC SB, Russian Academy of Sciences, Krasnoyarsk, Russia
[2] Federal Research Center KSC of Siberian Branch of RAS, Krasnoyarsk, Russia

E-mail: dabalaev@iph.krasn.ru

Received June 25, 2025
Revised July 28, 2025
Accepted July 28, 2025

The static magnetic properties of a system of $NiFe_2O_4$ nanoparticles (average size 4.5 nm) coated with polyvinyl alcohol (PVA) were studied. The analysis of the magnetization curves allowed us to conclude that the small particle size causes a pronounced „core/shell“ structure with structural and magnetic order in the core and, accordingly, disorder in the particle shell. The thickness of the disordered surface layer is ≈ 1 nm, and the ferrimagnetic core can only be formed in particles of about 4 nm or more in size. The coating of the particles leads to their spatial separation and a decrease in the intensity of magnetic interparticle interactions, which follows from a comparison with the data for a reference sample with identical particle sizes without PVA coating. The weakening of magnetic interparticle interactions is manifested in a decrease in the superparamagnetic blocking temperature of the magnetic moments of the particles caused by the ferrimagnetically ordered core. Another important consequence of the spatial separation of particles is the collapse of the common integrated surface for a cluster of particles, which is realized in the reference sample. This is manifested in a smaller value of the coercive force of the magnetic hysteresis loop (at $T = 4.2$ K) of the studied system of particles coated with PVA. Also, the paper discusses the processes of freezing of atomic magnetic moments located in disordered areas of particles.

Keywords: nickel ferrite, nanoparticles, magnetic interparticle interactions.

DOI: 10.61011/PSS.2025.09.62354.170-25

1. Introduction

Interest to magnetic nanoparticles is caused by capabilities of their practical application in various science-intensive technologies in biomedicine [1], chemical industry [2,3], microelectronics [4], instrumentation engineering [5] and other fields [6]. At the same time, at least two aspects are important: a small size of individual particles and new properties that appear in nanoscale particles. It is obvious that the new properties are a result of surface and dimension effects that are manifested in the nanoscale. However, there is another important effect, which in some cases crucially affects magnetic properties of nanoparticle systems. It is magnetic interparticle interactions (MII) [7–16]. In each specific practical application, it is important to understand which role is played by MIIs in the used material and, then, to optimize MII intensity for the required integral magnetic characteristics of the used system.

It is obvious that powder systems have MIIs, since the nanoparticles directly contact each other. MII intensity is determined not only by a value of magnetic moments of the particles and a distance between them, but properties of a nanoparticle surface as well [9,17–24]. It is possible to adjust MIIs by coating the particle surface with a weakly magnetic substance, thereby providing spatial separation of the particles [14,16,17,19–27].

The subject of the present study is a system of ultra-small (4−5 nm) nanoparticles of nickel ferrite $NiFe_2O_4$, which are coated by polyvinyl alcohol (PVA). The said small size for the oxide particles usually induces a pronounced structure of the particles of the „core/shell“ type [28] due to a large influence of a structure- and magnetically-disordered surface layer of the particles. That is why it is interesting to change magnetic characteristics of an ensemble of the nanoparticles of such ultra-small sizes during spatial separation of the particles. Results of characterization and detail study of the magnetic properties of the initial sample of the $NiFe_2O_4$ nanoparticles (uncoated) are given in the study [28], while it is shown in the study [23] that a value of the superparamagnetic (SPM) blocking temperature is significantly affected by the MIIs. We also note that the initial powder of nickel ferrite (with similar sizes of the particles) with uncoated particles exhibits effective heating in a mode of ferromagnetic resonance [29] (the so-called magnetic resonance hyperthermia [29–33]). The present study is aimed and revealing the effect of a coating of the $NiFe_2O_4$ nanoparticles on modification of the static magnetic properties of the system of such particles.

2. Experiment

The initial sample of the powder system of the $NiFe_2O_4$ nanoparticles was produced by chemical deposition after mixing initial components in water [28,29], without subsequent annealing. For comparison, the present study will provide temperature and field dependences of magnetization of this initial sample that is designated in accordance with the formula $NiFe_2O_4$.

The sample of the $NiFe_2O_4$ nanoparticles with addition of PVA was similarly produced with mixing the components in a 0.1% solution of polyvinyl alcohol [33]. The described procedure of preparation means particles sizes that are identical with the $NiFe_2O_4$ initial sample. Hereinafter this sample is designated as $NiFe_2O_4$/PVA.

The X-ray diffraction pattern of the produced samples exhibits only peaks that correspond to the $NiFe_2O_4$ structure. The average size of the particles $\langle d \rangle$, which is obtained by analysis of images of transmission electron microscopy (TEM) is ≈ 4 nm; the maximum size does not exceed 6 nm [28]. The obtained value of $\langle d \rangle$ agrees with the size of a coherent scattering region estimated from X-ray diffraction data using the Debye-Scherrer formula (≈ 3.5 nm) [28,29].

The temperature $M(T)$ (in the external fields $1-10$ kOe) and field $M(H)$ dependences of magnetization are measured on vibration sample magnetometer [34]. The dependences $M(T)$ in the fields 2, 100 and 500 Oe are measured on SQUID magnetometer [35]. For the temperature dependences, we have used regimes of zero field cooling (ZFC) and cooling in the external field (FC) from the temperature that significantly exceeds the value of the SPM blocking temperature.

3. Results and discussion

3.1. Dependences $M(T)$. Manifestation of the processes of SPM blocking and freezing magnetic subsystems

The dependences $M(T)$ in the ZFC and FC conditions in the field $H = 2$ Oe for the samples $NiFe_2O_4$ and $NiFe_2O_4$/PVA are shown in Figure 1, *a* and *b*, respectively. The following specific features of these dependences are worth noting. For the $NiFe_2O_4$ sample, the pronounced maxima of the dependence $M(T)$ in the ZFC conditions are observed at the temperatures ≈ 38 K and ≈ 7.6 K. The influence of a thermomagnetic history is manifested around the high-temperature maximum (a difference in magnetization for the ZFC and FC regimes appears). It is proven in the study [28] that the maximum of the dependence $M(T)_{ZFC}$ at the temperature of 38 K corresponds to SPM blocking of magnetic moments of the particles (hereinafter T_B is the SPM blocking temperature), while the low-temperature maximum reflects a transition of atomic (Fe^{3+}, Ni^{2+}) magnetic moments in the structurally-disordered small particles into a state of the spin glass type. Hereinafter, the temperature of this maximum is referred to as T_S. For the $NiFe_2O_4$/PVA sample, see Figure 1, *b*, the low-temperature maximum (the value of T_S is ≈ 9 K) became more pronounced, while the second maximum of the dependence $M(T)_{ZFC}$ was shifted to the temperature ≈ 19 K and became weakly pronounced. The influence of the thermomagnetic prehistory for the $NiFe_2O_4$/PVA sample starts from the temperature $T_{irr} \approx 24$ K, thereby making it possible to identify the temperature of ≈ 19 K as the SPM blocking temperature T_B, which reduced by ≈ 20 K as compared to the $NiFe_2O_4$ sample. It is natural to relate the observed decrease of the blocking temperature after spatial separation to attenuation of the MII influence, which was observed for various systems of magnetic nanoparticles [10,13–16,19–22,24–26].

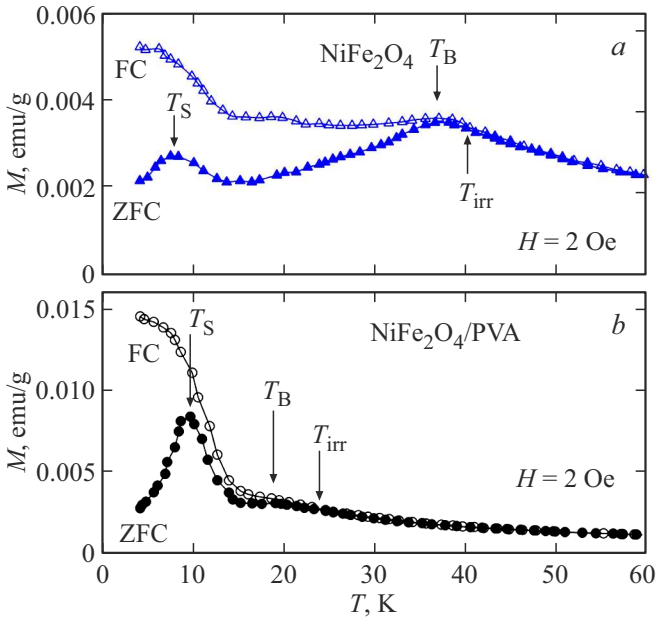

Figure 1. Temperature dependences of magnetization $M(T)$ in the ZFC and FC conditions in the external field $H = 2$ Oe for the samples $NiFe_2O_4$ (*a*) and $NiFe_2O_4$/PVA (*b*). They include temperatures that correspond to maximums of the dependences $M(T)_{ZFC}$: SPM blocking T_B, the temperature of freezing the subsystem of atomic magnetic moments T_S and the temperature of start of an irreversible behavior of magnetization T_{irr}.

The SPM blocking temperature usually decreases with the increase of the external field [10,13,19,21,23]. For the $NiFe_2O_4$ sample, the dependence $T_B(H)$ was analyzed within the framework of the model taking into account MIIs in the nanoparticle system [23]. At the same time, the resultant dependence $M(T)$ within the low temperatures is made up of contributions by (1) the particle blocking processes and (2) freezing the atomic magnetic moments (the maximum at the temperature T_S). For the $NiFe_2O_4$/PVA sample, the maximum at T_B becomes much less pronounced with the increase of the external field. It can be seen from data of Figure 2, which shows the dependences $M(T)/H$ in the ZFC conditions. In the fields that exceed the value of ~ 0.5 kOe, the dependences $M(T)_{ZFC}$ already do not

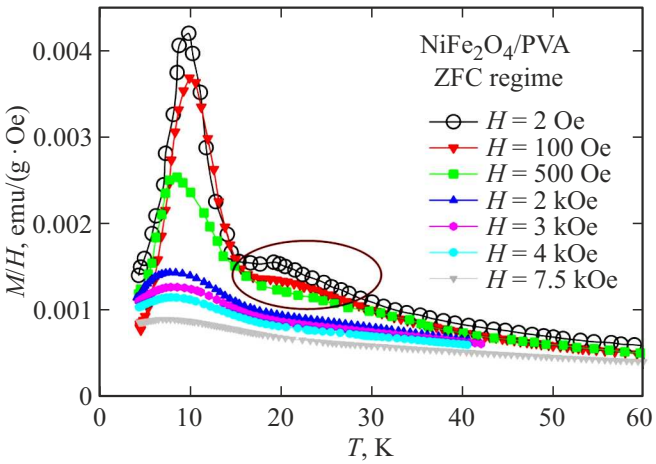

Figure 2. Temperature dependences of magnetization $M(T)/H$ in the ZFC conditions for the $NiFe_2O_4$/PVA in the different external fields (they are specified in the legend). An (oval-)selected area on the dependences $M(T)$ exhibits specific features that correspond to the SPM blocking processes.

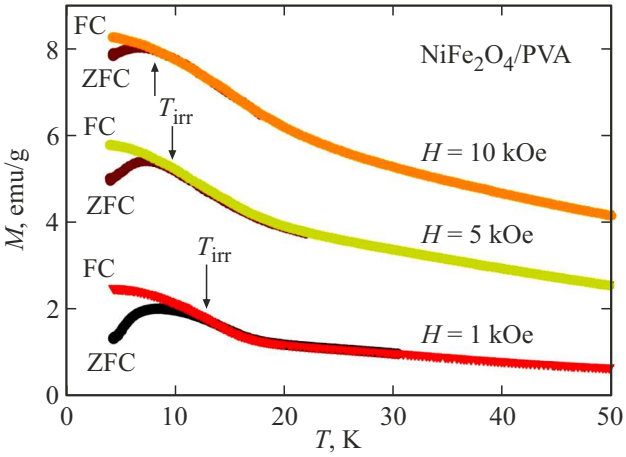

Figure 3. Temperature dependences of magnetization $M(T)$ in the ZFC and FC conditions for the $NiFe_2O_4$/PVA sample in the external fields $H = 1$, 5 and 10 kOe. It shows the temperatures of start of the irreversible behavior of magnetization T_{irr}.

exhibit a maximum at T_B; the maximum of the curve is shifted into the low-temperature area, which is dominated by a contribution by the process of freezing the atomic magnetic moments. It is indirectly supported by the fact that within the range of the fields 1–10 kOe the temperature of start of the irreversible behavior of magnetization T_{irr} is noticeably shifted into the low temperatures — from ≈ 13 K ($H = 1$ kOe) to ≈ 8 K ($H = 10$ kOe) (Figure 3).

Thus, the following conclusions can be made based on analysis of the behavior of the temperature dependences of magnetization and their comparison with similar data for the sample with the uncoated particles. Both the samples exhibit magnetic contributions from at least two magnetic subsystems, one of them is magnetic moments of the particles (it transits into the SPM state at the temperature T_B), while the other is a subsystem of the atomic magnetic moments, which is frozen (or transits into the state of the spin glass type) when $T = T_S$. The SPM blocking temperature for the $NiFe_2O_4$/PVA sample decreased in two times and is ≈ 19 K, which is a manifestation of the decrease of MII intensity. At the same time, the value of the temperature T_S is slightly changed (≈ 7.6 K for the $NiFe_2O_4$ sample and ≈ 9 K for the $NiFe_2O_4$/PVA sample). It additionally supports the previous conclusions [28] that at the low temperature the atomic magnetic moments in the structurally-disordered small particles transit into the state of the spin glass type; and the additional coating of the particles does not result in significant changes in these processes.

3.2. Analysis of the magnetization curves, selection of contributions by the magnetic subsystems

The magnetization curves of the $NiFe_2O_4$/PVA sample, which are measured within the temperatures 100–250 K, within which the magnetic moments of the particles are in the SPM state, are shown in Figure 4, *a*. The SPM behavior of magnetization is usually modelled by the Langevin function $L(\mu_P, H) = \coth(\mu_P \cdot H/kT) - 1/(\mu_P \cdot H/kT)$, where μ_P is the magnetic moment of the particle, k is the Boltzmann's constant. It is clear from the shape of the dependences $M(H)$ that the quite high fields have a noticeably contribution by a field-linear response of magnetization. Consequently, describing the curves of magnetization requires to use a superposition of the Langevin function and the field-linear function, which is hereinafter referred to as $\chi_{PM}H$, where $\chi_{PM} = \text{const}$. Taking into account a distribution along the magnetic moments of the particles $f(\mu_P)$ results in the following expression for processing experimental dependences $M(H)$:

$$M(H) = N_P \int_0^\infty \mathrm{L}(\mu_P, \mathrm{H}) f(\mu_P) \mu_P d\mu_P + \chi_{PM}\mathrm{H}. \qquad (1)$$

In this expression, N_P is a number of the particles in a unit mass of the sample, the lognormal distribution $f(\mu_P) = (\mu_P \cdot s \cdot (2\pi)^{1/2})^{-1} \exp\{-[\ln(\mu_P/n)]^2/2s^2\}$ is used as $f(\mu_P)$, in which $\langle\mu_P\rangle$ is an average magnetic moment per the particle $(\langle\mu_P\rangle = n \cdot \exp(s^2))$, s^2 is dispersion of the magnitude $\ln(\mu_P)$. During the procedure of the experimental dependences $M(H)$, the values of N_P and s were fixed (were not changed for the various temperatures), and only the parameters n (actually, this is the value of $\langle\mu_P\rangle$) and χ_{PM} varied with the temperature. The results of the best fitting of the dependences $M(H)$ are shown in Figure 4, *a* by solid lines. The values of N_P and s are given in Table. Partial components of the fitting curves, i. e. the first and second terms of the expression (1): $M_{SPM}(H)$ are $M_{PM}(H) = \chi_{PM} \cdot H$ shown in Figure 4, *b*.

Evolution of the distribution function $f(\mu_P)$ at the various temperatures is shown in Figure 5. The temperature

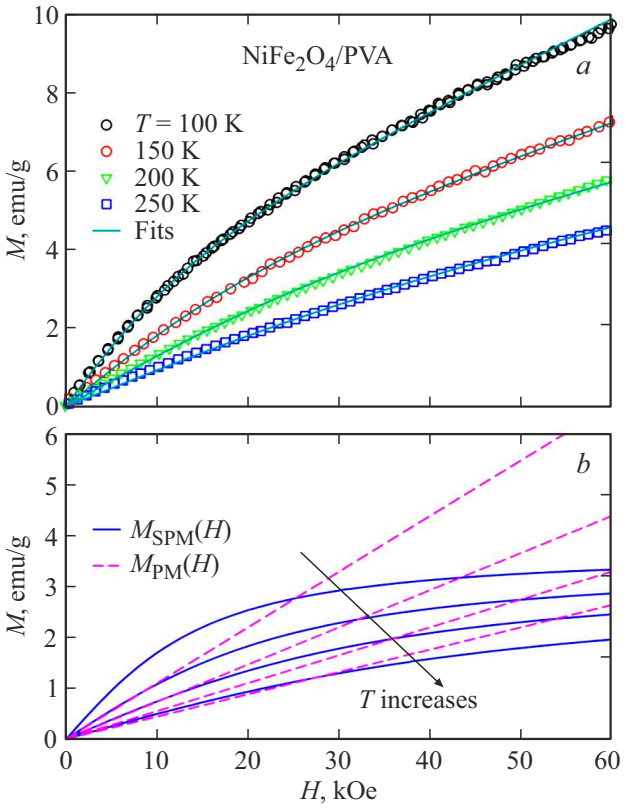

Figure 4. *a* — experimental (symbols) dependences $M(H)$ at the legend-specified temperatures and results of the best fitting as per the expression (1); *b* — partial components (the first — $M_{FM}(H)$ and second — $M_{PM}(H)$ terms of the expression (1)) of the fitting curves $M(H)$.

dependences of the main fitting parameters $\langle\mu_P\rangle$ and χ_{PM} are shown in Figure 6. The obtained values of $\langle\mu_P\rangle$ at the various temperatures are quite well described by the expression

$$\langle\mu_P\rangle = \langle\mu_P\rangle(T=0)\cdot(1-AT^{\alpha}), \qquad (2)$$

where α and A are constants. The best agreement is achieved when the value $\alpha = 1.5\pm0.1$ and the value $\langle\mu_P\rangle(T=0)\approx 236\cdot\mu_B$ (μ_B — is a Bohr magneton). The distribution of $f(\mu_P)$ when $T=0$ in Figure 5 is obtained for the said extrapolated magnitude $\langle\mu_P\rangle(T=0)$ and the unchanged parameters N_P and s (Table). In turn, the values of $\chi_{PM}(T)$ vary with the temperature as $1/T$ (Figure 6), i. e. the following relationship is fulfilled in the temperature interval above 100 K

$$\chi_{PM}(T) = C_{PM}\cdot(1/T), \qquad (3)$$

in which $C_{PM}\approx 0.011\,(\text{emu}\cdot\text{K})/(\text{g}\cdot\text{Oe})$.

Let us compare the obtained values of the fitting parameters with similar parameters for the $NiFe_2O_4$ initial sample [28] (see Table). The parameters s of the lognormal distribution turned out to be the same and values of the average magnetic moment of the particles $\langle\mu_P\rangle(T=0)$ turned out to be close. The number of the particles N_P per gram of the $NiFe_2O_4$/PVA sample is less than in the $NiFe_2O_4$ sample by a multiplier $m\approx 0.73$ and the values of C_{PM} differ by the same multiplier. It is estimated in the first approximation that the weight percentage of PVA in the $NiFe_2O_4$/PVA sample is about 27 wt.% or its volume content exceeds 50%. The listed facts indirectly indicate that the distributions $f(\mu_P)$ are similar in the samples $NiFe_2O_4$/PVA and $NiFe_2O_4$.

The value of M_{SPM}, which is specified in Table, is actually saturation magnetization of the SPM contribution when $T=0$. The magnitude M_{SPM} is related to the average magnetic moment of the particle by a relationship $M_{SPM} = N_P\langle\mu_P\rangle$. The value of $M_{SPM}(T=0)$ for the $NiFe_2O_4$/PVA sample, which is reduced to the weight of nickel ferrite (taking into account the multiplier $m\approx 0.73$), is ≈ 5.5 emu/g. It is somewhat lower, but quite close to the value of $M_{SPM}(T=0)$ of the $NiFe_2O_4$ sample. However, for

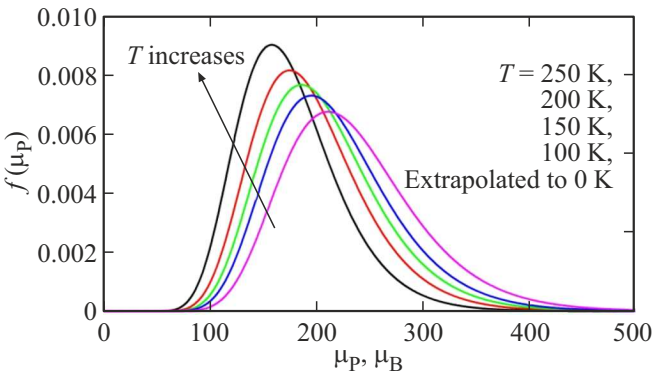

Figure 5. Distribution function $f(\mu_P)$ at the various temperatures, which is used for fitting the magnetization curves $M(H)$ (Figure 4, *a*). For $f(\mu_P)$ when $T=0$, we used the extrapolated value of $\langle\mu_P\rangle(T=0)$ and the parameters N_P and s, which are given in Table.

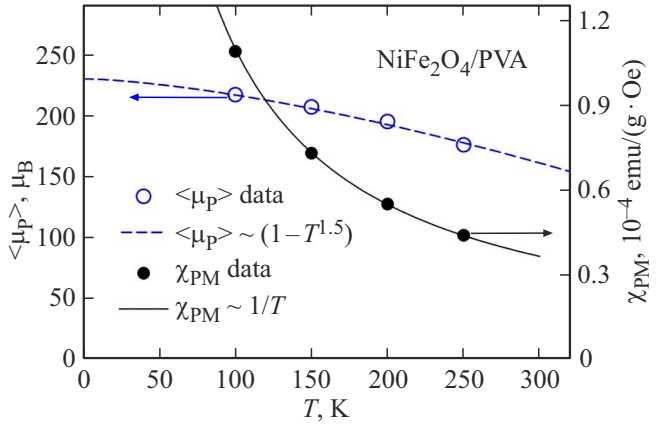

Figure 6. Temperature evolution of the average magnetic moment of the particles $\langle\mu_P\rangle$ (the left ordinate axis) and the value of χ_{PM} (the right ordinate axis). The solid curves are calculated by the expressions (2) and (3).

Parameter s of the lognormal distribution $f(\mu_P)$, the values of N_P, $\langle\mu_P(T=0)\rangle$, $M_{SPM}(T=0)$ and C_{PM}, which are reduced with the sample weight and obtained for the fitting dependences $M(H)$ (Figure 4)

Sample	s	N_P, particle/g	$\langle\mu_P\rangle(T=0)$, μ_B	$M_{SPM}(T=0)$, emu/g	C_{PM}, (emu · K)/(g · Oe)
$NiFe_2O_4$/PVA	0.27 ± 0.02	$1.81 \cdot 10^{18}$	236	4.0	0.011
$NiFe_2O_4$ [28]	0.27 ± 0.02	$2.48 \cdot 10^{18}$	296	6.8	0.015

both the samples, $M_{SPM}(T=0)$ is significantly less than the respective value of bulk $NiFe_2O_4$ ($M_{Sbulk} \approx 51$ emu/g [36]).

A decrease of saturation magnetization for the nanoscale ferro- and ferri-magnetic particles is related to presence of a structurally-disordered layer on the particle surface, which has not magnetic ordering [28,37–43]. This subsurface layer is termed as a „magnetic-dead" layer. The thickness d_{md} of this layer can be evaluated from simple geometrical considerations. The particle of the volume V has a ferrimagnetically-ordered „core" of the volume V_{CORE} and a disordered surface of the volume V_{SHELL}, $V = V_{CORE} + V_{SHELL}$. It follows from the obvious relationship $M_{SPM}/M_{Sbulk} = V_{CORE}/V$ that

$$M_{SPM} = M_{Sbulk} \cdot (1 - 2 \cdot d_{md}/d)^3, \qquad (4)$$

from which, when $d = \langle d\rangle \approx 4.0$ nm, we obtain that $d_{md} \approx 1$ nm. For this value of d_{md}, the particle of the size of 2 nm will be fully „non-magnetic", while at the higher sizes the ferrimagnetically-ordered core can be formed only when it has a volume of several lattice cells of $NiFe_2O_4$. Actually, the ferrimagnetically-ordered core is formed only in the particles of the size of at least 4 nm.

The above said is confirmed by recalculation of the distribution function $f(\mu_P)$ (determined from the condition of the best fitting, with the value of $\langle\mu_P\rangle$ extrapolated to $T=0$) into a size distribution and its comparison with the distribution $f(d)$ that is obtained from TEM data. For ideally ordered particles of nickel ferrite $\mu_P \approx N_{FU} \cdot 2.3\,\mu_B$ [44], where N_{FU} is a number of formula units in the particle. Using a value of the averaged distance d_{am} between magnetically active ions in $NiFe_2O_4$ ($d_{am} \approx 0.35$ nm [45]), the following relationship can be obtained:

$$\mu_P \approx (1/3) \cdot [d^*/d_{am} + 1]^3 \cdot 2.3\,\mu_B. \qquad (5)$$

Here, d^* is a size of the ordered core of the particle and in our case $d^* = d - 2 \cdot d_{md}$. Along with a histogram of the particle size distribution, Figure 7 also shows distributions $f(d = d^* + 2 \cdot d_{md})$ of the samples $NiFe_2O_4$/PVA and $NiFe_2O_4$, which are obtained by means of the expression (5). Hatched columns in the histogram correspond to the particles that have ferrimagnetic ordering in the particle „core" and the magnetic moment μ_P. It is clear that the dependences $f(d)$ well agree with the histogram of the size distribution within the range $d > 4$ nm, thereby additionally confirming lack of the magnetic order in the „small" ($d < 4$ nm) particles and presence of the magnetic-dead layer in the „large" ($d > 4$ nm) particles. The „small" and „large" particles are also schematically represented in a field of Figure 7.

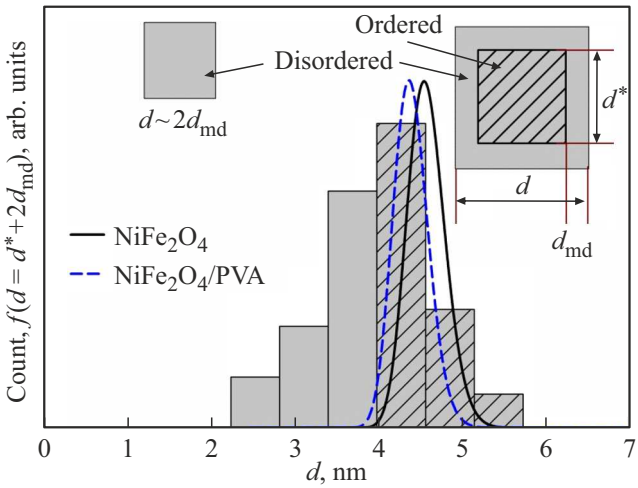

Figure 7. Histogram of the nanoparticle size distribution and the distribution $f(d = d^* + 2 \cdot d_{md})$, which are recalculated by the expression (5) from the distributions $f(\mu_P)$ (obtained from results of processing the dependences $M(H)$ — Figure 4, *a*) of the samples $NiFe_2O_4$/PVA and $NiFe_2O_4$. It also schematically represents the areas of the structural and magnetic order and disorder in the „small" ($d < 4$ nm) and „large" ($d > 4$ nm) particles.

If the SPM behavior is determined by the magnetic moment μ_P of the ferrimagnetically-ordered „core" of the particles, then it is logical to identify the magnetic response from spins in the surface layer d_{md} and spins of the small (< 4 nm) particles with the second summand of the expression (1). The paramagnetic behavior of the dependence $\chi_{PM}(T)$ (the expression (3)) indicates that within the high temperatures (above 100 K) this magnetic subsystem is not associated with the subsystem of the ferrimagnetically-ordered „cores" of the particles. With the decrease of the temperature, when $T_S \approx 9$ K, this subsystem is frozen and transits into the state of the spin glass type (Figure 2).

It was shown in the study [28] that for the $NiFe_2O_4$ initial sample, in which the particles directly contact each other, some surface spins are frozen somewhat earlier — within the interval between the temperatures T_S and T_B. And we are talking mainly about the magnetic moments of the atoms on the surface of the particles, whose sizes exceed 4 nm.

Actually, presence of three magnetic subsystems was stated for the $NiFe_2O_4$ sample: (i) the ferrimagnetically-ordered core of the „large“ ($d > 4$ nm) particles, (ii) spins of the common (for the particle cluster) integrated surface of the „large“ ($d > 4$ nm) particles, and (iii) spins of the atoms in the disordered „small“ ($d < 4$ nm) particles. The magnetic moments μ_P of the subsystem (i) are blocked at the temperature T_B, the spins of the subsystem (ii) are frozen within the interval $T_B - T_S$ (without manifesting outstanding specific features on the temperature dependences of static magnetization), and the spins of the subsystem (iii) are frozen around the temperature T_S [28].

By comparing values of the magnetic response of the samples $NiFe_2O_4$/PVA and $NiFe_2O_4$ within the area of the low-temperature maximum (Figure 1), it can be seen that M_{ZFC} in the point of the maximum, i.e. the value of $M(T = T_S)_{ZFC}$, is noticeably higher for the $NiFe_2O_4$/PVA sample. A relative change of magnetization around a low-temperature „bell“ is also higher, when comparing, for example, values of the difference $\Delta M = M(T = T_S)_{ZFC} - M(T = 4.2\,\mathrm{K})_{ZFC}$. It can be explained within the framework of the following scenario. The $NiFe_2O_4$/PVA sample already has not the common integrated surface for the cluster of the „large“ ($d > 4$ nm) particles, and the subsystems (ii) and (iii) are united into a single subsystem, which is frozen at the temperature T_S. Then, for the $NiFe_2O_4$/PVA sample, with a decrease of the temperature there will be an increase of magnetization by this subsystem (ii + iii) to the temperature T_S as per a functional dependence that is close to the expression (3). In turn, the spins of the subsystem (ii) are frozen earlier for the $NiFe_2O_4$ sample — within the interval between T_B and T_S, and only the spins of the subsystem (iii) are frozen around the temperature T_S, thereby resulting in a smaller value of magnetization $M(T = T_S)_{ZFC}$ and of the magnitude of the difference $M(T = T_S)_{ZFC} - M(T = 4.2\,\mathrm{K})_{ZFC}$.

The framework of the described scenario is used to explain the smaller value of the coercive force H_C of the $NiFe_2O_4$/PVA sample as compared to the $NiFe_2O_4$ initial sample. It is clear from data of Figure 8 (the full loops of magnetic hysteresis) and its lower insert (the dependences $M(H)$ around the origin of coordinates). The values of H_C when $T = 4.2$ K are ≈ 1.5 and ≈ 2.6 kOe for the $NiFe_2O_4$/PVA sample and the $NiFe_2O_4$ sample, respectively. Hysteresis of the magnetization curve is a typical specific feature of single-domain magnetic nanoparticles, whose magnetic moments are in a blocked state. The magnitude H_C is determined by a ratio of magnitudes of a magnetic anisotropy constant and saturation magnetization, and these characteristics are approximately the same for individual particles of the samples $NiFe_2O_4$/PVA and $NiFe_2O_4$. Then, the higher value of H_C for the $NiFe_2O_4$ sample can be explained by the influence of the common integrated surface of the particle cluster, more exactly, by the influence of a relation of the magnetic subsystems (i) and (ii). Actually, it is required to remagnetize the two related magnetic subsystems in the $NiFe_2O_4$ sample, while

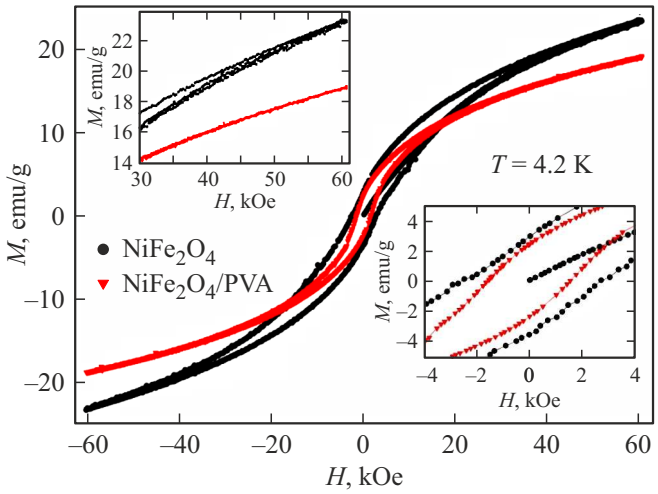

Figure 8. Loops of magnetic hysteresis $M(H)$ of the samples $NiFe_2O_4$/PVA and $NiFe_2O_4$ at $T = 4.2$ K. The insert includes the same around the origin of coordinates. The upper insert includes portions of the dependence $M(H)$ within the fields of above 30 kOe.

magnetic moments of separate particles are remagnetized in the $NiFe_2O_4$/PVA sample. It results in a higher value of the coercive force of the $NiFe_2O_4$ initial sample. The above said is additionally confirmed by a difference in values of the field of the irreversible behavior of magnetization of the samples (Figure 8, the upper insert). If for the $NiFe_2O_4$/PVA sample hysteresis of magnetization becomes vanishingly small in the external field of ~ 40 kOe, then for the $NiFe_2O_4$ sample at the maximum used field of 60 kOe the loop of hysteresis is still open.

4. Concluding remarks

The static magnetic properties of the $NiFe_2O_4$/PVA sample are studied and compared with the properties of the $NiFe_2O_4$ initial sample to make the following conclusions.

Addition of PVA at one of stages of synthesis of the ferrite powder results in spatial separation of the particles and reduction of MII intensity. The latter is manifested in reduction of the temperature of SPM blocking of the magnetic moments of the particles from 38 to 19 K.

Both the powder systems are characterized by the structure of the particles of the „core/shell“ type, which includes structural and magnetic ordering in the „core“ of the particles, while the surface layer of the thickness of about 1 nm is disordered. However, here, we are talking about the quite „large“ particles, whose size d exceeds 4 nm. The particles of the size of less than 4 nm are fully disordered.

Besides, both the ferrite powder systems have identical size distributions of the magnetic moments of the particles and values of the SPM contribution. The magnetic moment of the particles, which induces the SPM behavior at the

high temperatures, is determined by the ferrimagnetically-ordered „core“ of the particles.

For the $NiFe_2O_4$/PVA sample, the atomic magnetic moments of the „small“ ($d < 4\,\text{nm}$) particles and the disordered surface layer of the „large“ ($d > 4\,\text{nm}$) particles are frozen within the low temperatures when $T_S \approx 9\,\text{K}$. At the same time, for the $NiFe_2O_4$ initial sample we have recorded the difference of the magnetic properties of the common integrated surface for the „large“ ($d > 4\,\text{nm}$) particles, in which the atomic magnetic moments are frozen within the temperature interval $T_S - T_B$, and of the magnetic subsystem in the „small“ ($d < 4\,\text{nm}$) particles with the freezing temperature of $\approx 7.6\,\text{K}$. It is obvious that spatial separation of the particles, which is realized in the $NiFe_2O_4$/PVA sample, results in a collapse of the common integrated surface, which is manifested in reduction of the coercive force.

Acknowledgments

The authors would like to thank Yu.V. Knyazev for fruitful discussions.

Funding

The study was carried out within the framework of the state assignment of Institute of Physics, Siberian Branch of RA, and the sample was prepared within the framework of the state assignment of Federal Research Center KSC of Siberian Branch of RAS.

Conflict of interest

The authors declare that they have no conflict of interest.

References

[1] H.A. Khan, M.K. Sakharkar, A. Nayak, U. Kishore, A. Khan. Nanobiomaterials **2018**, 357 (2018).
[2] M. Amiri, M. Salavati-Niasari, A. Akbari. Adv. Colloid Interface Sci. **265**, 29 (2019).
[3] Ali, T. Shah, R. Ullah, P. Zhou, M. Guo, M. Ovais, Z. Tan, Y. Rui. Front. Chem. **9**, 629054 (2021).
[4] S. Ohkoshi, A. Namai, K. Imoto, M. Yoshikiyo, W. Torora, K. Nakagawa, M. Komine, Y. Miyamoto, T. Nasu, S. Oka, H. Tokoro. Sci. Rep. **5**, 14414 (2015).
[5] A. Namai, M. Yoshikiyo, K. Yamada, S. Sakurai, T. Goto, T. Yoshida, T. Miyazaki, M. Nakajima, T. Suemoto, H. Tokoro, S. Ohkoshi. Nat. Commun. **3**, 1035 (2012).
[6] X. Batlle, C. Moya, M. Escoda-Torroella, Ò. Iglesias, A.F. Rodríguez, A. Labarta. J. Magn. Magn. Mater. **543**, 168594 (2022).
[7] C. Djurberg, P. Svedlindh, P. Nordblad, M. F. Hansen, F. Bødker, S. Mørup. Phys. Rev. Lett. **79**, (N25) 5154 (1997).
[8] G.F. Goya, T.S. Berquó, F.C. Fonseca, M.P. Morales. J. Appl. Phys. **94**, 3520 (2003).
[9] S. Mørup, D.E. Madsen, C. Fradsen, C.R.H. Bahl, M.F. Hansen. J. Phys.: Condens. Matter **19**, 213202 (2007).
[10] J.M. Vargas, W.C. Nunes, L.M. Socolovsky, M. Knobel, D. Zanchet. Phys. Rev. B **72**, 184428 (2005).
[11] M. Suzuki, S.I. Fullem, I.S. Suzuki, L. Wang, Ch.-J. Zhong. Phys. Rev. B **79**, 024418 (2009).
[12] S.V. Komogortsev, V.A. Fel'k, O.A. Li. J. Magn. Magn. Mater. **473**, 410 (2019).
[13] W.C. Nunes, L.M. Socolovsky, J.C. Denardin, F. Cebollada, A.L. Brandl, M. Knobel. Phys. Rev. B **72**, 212413 (2005).
[14] M. Knobel, W.C. Nunes, H. Winnischofer, T.C.R. Rocha, L.M. Socolovsky, C.L. Mayorga, D. Zanchet. Journal of Non-Crystalline Solids **353**, 743 (2007).
[15] F. Fabris, Kun-Hua Tu, C.A. Ross, W.C. Nunes. J. Appl. Phys. **126**, 173905 (2019).
[16] C.A.M. Vieira, R. Cabreira Gomes, F.G. Silva, A.L. Dias, R. Aquino, A.F.C. Campos, J. Depeyrot. J. Phys.: Condens. Matter **31**, 17580 (2019).
[17] T.S. Berquó, J.J. Erbs, A. Lindquist, R.L. Penn, S.K. Banerjee. J. Phys.: Condens. Matter **21**, 176005 (2009).
[18] K. Nadeem, M. Kamran, A. Javed, F. Zeb, S.S. Hussain, M. Mumtaz, H. Krenn, D.V. Szabo, U. Brossmann, X. Mu. Solid State Sciences **83**, 43 (2018).
[19] A.A. Krasikov, Yu.V. Knyazev, D.A. Balaev, S.V. Stolyar, V.P. Ladygina, A.D. Balaev, and R.S. Iskhakov, JETP **137** (N. 6), 903 (2023).
[20] Yu.V. Knyazev, D.A. Balaev, S.A. Skorobogatov, D.A. Velikanov, O.A. Bayukov, S.V. Stolyar, R.N. Yaroslavtsev, R.S. Iskhakov. Phys. Rev. B **107**, 115413 (2023).
[21] D.A. Balaev, A.A. Krasikov, S.V. Stolyar, R.N. Yaroslavtsev, S.A. Skorobogatov, D.A. Velikanov, R.S. Iskhakov. Physics of the Solid State **66**, *11*, 1829 (2024).
[22] Yu.V. Knyazev, D.A. Balaev, S.A. Skorobogatov, D.A. Velikanov, O.A. Bayukov, S.V. Stolyar, V.P. Ladygina, A.A. Krasikov, and R.S. Iskhakov. Physics of Metals and Metallography, **125**, *4*, 377 (2024).
[23] D.A. Balaev, A.A. Krasikov, Yu.V. Knyazev, S.V. Stolyar, A.O. Shokhrina, A.D. Balaev*, and R.S. Iskhakov. JETP Letters **120**, *10*, 751 (2024).
[24] D.A. Balaev, A.A. Krasikov, S.A. Skorobogatov, S.V. Stolyar, R.N. Yaroslavtsev, R.S. Iskhakov. JETP Letters **122**, *1*, 48 (2025).
[25] D. Caruntu, G. Caruntu, Ch.J. O'Connor. J. Phys. D: Appl. Phys. **40**, 5801 (2007).
[26] D.A. Balaev, S.V. Semenov, A.A. Dubrovskiy, S.S. Yakushkin, V.L. Kirillov, O.N. Martyanov. J. Magn. Magn. Mater. **440**, 199 (2017).
[27] M. Vasilakaki, F. Gemenetzi, E. Devlin, D.K. Yi, S.N. Riduan, S.S. Lee, J.Y. Ying, G.C. Papaefthymiou, K.N. Trohidou. J. Magn. Magn. Mater. **522**, 167570 (2021).
[28] Yu.V. Knyazev, D.A. Balaev, S.V. Stolyar, A.O. Shokhrina, D.A. Velikanov, A.I. Pankrats, A.M. Vorotynov, A.A. Krasikov, S.A. Skorobogatov, M.N. Volochaev, O.A. Bayukov, R.S. Iskhakov. J. Magn. Magn. Mater. **613**, 172675 (2025).
[29] S.V. Stolyar, O.A. Li, E.D. Nikolaeva, N.M. Boev, A.M. Vorotynov, D.A. Velikanov, R.S. Iskhakov, V.F. P.yankov, Yu.V. Knyazev, O.A. Bayukov, A.O. Shokhrina, M.S. Molokeev, A.D. Vasil'ev. Physics of the Solid State **65**, *6*, 963 (2023).
[30] S.V. Stolyar, O.A. Li, E.D. Nikolaeva, A.M. Vorotynov, D.A. Velikanov, Yu.V. Knyazev, O.A. Bayukov, R.S. Iskhakov, V.F. P'yankov, M.N. Volochaev. Physics of Metals and Metallography, **124**, *2*, 174 (2023).

[31] S.V. Stolyar, O.A. Li, A.M. Vorotynov, D.A. Velikanov, N.G. Maksimov, R.S. Iskhakov, V.P. Ladygina, A.O. Shokhrina. Bulletin of the Russian Academy of Sciences: Physics **88**, 536 (2024).
[32] S.V. Stolyar, E.D. Nikolaeva, O.A. Li, D.A. Velikanov, A.M. Vorotynov, V.F. Pyankov, V.P. Ladygina, A.L. Sukhachev, D.A. Balaev, R.S. Iskhakov. Inorganic Materials: Applied Research **15**, 927 (2024).
[33] S.V. Stolyar, I.G. Vazhenina , A.O. Shokhrina, E.D. Nikolaeva, O.A. Li, R.S. Iskhakov, A.V. Belyi. Physics of the Solid State **67**, *7*, 1273 (2025).
[34] A.D. Balaev, Y.V. Boyarshinov, M.M. Karpenko and B.P. Khrustalev. Instrum. Exp. Tech.(Engl. Transl.); (United States), **26**, N3, (1985).
[35] D.A. Velikanov. Siberian Aerospace Journal **14**, no. 2, 176, (2013).
[36] R.H. Kodama, A.E. Berkowitz, E.J. McNiff, S. Foner. J. Appl. Phys. **81**, 5552 (1997).
[37] R.J. Tackett, A.W. Bhuiya, C.E. Botez. Nanotechnology **20**, 445705 (2009).
[38] S. Mitra, K. Mandal, P. Anil Kumar. J. Magn. Magn. Mater. **306**, 254 (2006).
[39] A. Millan, A. Urtizberea, N.J.O. Silva, F. Palacio, V.S. Amaral, E. Snoeck, V. Serin. J. Magn. Magn. Mater. **312**, L5 (2007).
[40] A.P. Safronov, I.V. Beketov, S.V. Komogortsev, G.V. Kurlyandskaya, A.I. Medvedev, D.V. Leiman, A. Larrañaga, S.M. Bhagat. AIP Adv. **3**, 052135 (2013).
[41] D. Zákutná, D. Nižňanský, L.C. Barnsley, E. Babcock, Z. Salhi, A. Feoktystov, D. Honecker, S. Disch. Phys. Rev. X **10**, 031019 (2020).
[42] Li Wang, J. Li, M. Lu, H. Dong, J. Hua, S. Xu, H. Li. J. Supercond. Nov. Magn. **28**, 191 (2015).
[43] A.A. Krasikov, D.A. Balaev. JETP **136**, *1*, 97 (2023).
[44] Yu. Sitikhadze, Kh. Sato. Ferrity. Mir, M. (1964). 407 s. (in Russian).
[45] A. Adam, Z. Ali, E. Abdeltwab, Y. Abbas. Journal of Ovonic Research **5** (5), 157 (2009).

Translated by M.Shevelev